Geochemistry Geophysics Geosystems G3
AN ELECTRONIC JOURNAL OF THE EARTH SCIENCES
Published by AGU and the Geochemical Society

Article
Volume 7, Number 12
29 December 2006
Q12009, doi:10.1029/2006GC001410
ISSN: 1525-2027

Injection mechanism of clay-rich sediments into dikes during earthquakes

Tsafrir Levi
Department of Geological and Environmental Sciences, Ben Gurion University of the Negev, P.O. Box 653, Beer Sheva, Negev 84105, Israel

Geological Survey of Israel, 30 Malkhei Israel Street, 95501, Jerusalem, Israel

Ramon Science Center, Ben Gurion University of the Negev, P.O. Box 194, 80600, Mizpe Ramon, Israel (zafrir@bgumail.bgu.ac.il)

Ram Weinberger
Geological Survey of Israel, 30 Malkhei Israel Street, 95501, Jerusalem, Israel

Tahar Aïfa
Géosciences-Rennes, CNRS UMR6118, Université de Rennes l, Campus de Beaulieu, F-35042 Rennes Cedex, France

Yehuda Eyal
Department of Geological and Environmental Sciences, Ben Gurion University of the Negev, P.O. Box 653, Beer Sheva, Negev 84105, Israel

Shmuel Marco
Department of Geophysics and Planetary Sciences, Tel Aviv University, 69978, Tel Aviv, Israel

[1] Clastic dikes may form by simultaneous fracture propagation in rocks and injection of clastic material into the fractures resulting from strong seismic shaking. We studied the mechanisms of clastic-dike formation within the seismically active Dead Sea basin, where hundreds of clastic dikes cross-cut the soft rock of the late Pleistocene lacustrine Lisan Formation. We analyzed the anisotropy of magnetic susceptibility (AMS) of dikes with known formation mechanisms and defined the characteristic AMS signatures, mainly of dikes developed by injection process. Most of the dikes were emplaced due to fluidization of clay-rich sediment and are characterized by triaxial AMS ellipsoids. The dominant triaxial AMS ellipsoids along the dike widths suggest that the fluidization mechanism of clay-rich sediment is different from the known liquefaction process of sand. The AMS analysis supported by field evidence indicates that the injection of clay-rich sediment is characterized by two main regimes: (1) Vertical flow characterized by subvertical V_2 axes and subhorizontal V_1 and V_3 axes. The V_2 axes may indicate the flow directions during fast flow. (2) Horizontal slow flow characterized by subvertical V_3 axes and subhorizontal V_1 and V_2 axes. A streaked AMS pattern mainly composed of V_2 and V_3 axes represents a turbulent flow that generated local eddies simultaneously with the clastic transport. The AMS parameters along the dikes and possible grain imbrications along dike walls support organization of grains under high strain rates. This application of the AMS method provides a petrofabric tool for identifying seismites and inferring their flow kinematics in complex geologic areas.

Components: 9713 words, 13 figures.

Keywords: clastic dikes; fluid flow; anisotropy of magnetic susceptibility; Dead Sea Transform.

Index Terms: 1518 Geomagnetism and Paleomagnetism: Magnetic fabrics and anisotropy; 7221 Seismology: Paleoseismology (8036); 3653 Mineralogy and Petrology: Fluid flow.

Received 4 July 2006; **Revised** 27 August 2006; **Accepted** 18 September 2006; **Published** 29 December 2006.

Levi, T., R. Weinberger, T. Aïfa, Y. Eyal, and S. Marco (2006), Injection mechanism of clay-rich sediments into dikes during earthquakes, *Geochem. Geophys. Geosyst.*, *7*, Q12009, doi:10.1029/2006GC001410.

1. Introduction

[2] Paleoseismic records commonly document strong to very strong (magnitude, M > 6) earthquakes, whereas geologic evidence of small and moderate-sized earthquakes is rarely preserved at the surface. Recognition of seismic events in the stratigraphic record is important in order to characterize their frequency-size relations and complete the paleoseismic record [*McCalpin*, 1996; *Rodríguez-Pascua et al.*, 2000].

[3] Seismites are deformational structures attributable to seismic activity. Our study deals with injected clastic dikes which are discordant sheets of clastic sediments formed by forceful intrusion of fluidized clastic material into the surrounding strata. Injection clastic dikes are one form of seismites, and their emplacement corresponds to episodic pulses of increasing hydraulic pressure generated by seismic loading [*McCalpin*, 1996]. The pattern of injection dikes has been used for locating paleoepicenters [*Galli*, 2000, and references therein]. Noteworthy, determining a seismic origin of injection clastic dikes is not trivial because their appearance may be similar to that of depositional dikes, formed by passive infilling of fissures from above.

[4] Injection clastic dikes are referred to as liquefaction structures. Engineering studies of ground deformation associated with historical earthquakes have shown that near-surface water-saturated sediments become liquefied as a result of cyclical shear stress [*McCalpin*, 1996, and references therein]. The liquefaction occurs as a consequence of the increased pore water pressure whereby the granular porous material is transformed from a solid state into a liquefied state. Soft-sediment deformation is referred to as flowage or fluidization of cohesionless clay-rich sediments [*Mohindra and Bagati*, 1996]. Pore pressure may be involved as well, but little is known about its mechanism, especially during an earthquake shaking. Although unconsolidated sandy soils are considered to be materials that are most sensitive to liquefaction, clay-rich soils can also be fluidized during an earthquake. Several geological studies [e.g., *Mohindra and Bagati*, 1996; *Rodríguez-Pascua et al.*, 2000; *Moretti*, 2000] described soft-sediment structures and suggested that these structures were formed during earthquakes.

[5] In this study we apply anisotropy of magnetic susceptibility (AMS) analysis to characterize the seismic origin of injection dikes. Foliation and lineation of the magnetic fabric may form during transport, deposition and deformation of rocks [*Borradaile and Henry*, 1997]. The fabric is commonly associated with AMS, and can be used as an indicator for flow directions in sediments [*Tarling and Hrouda*, 1993; *Liu et al.*, 2001] and in magmas [*Baer*, 1995; *Aïfa and Lefort*, 2001; *Abelson et al.*, 2001; *Poland et al.*, 2004]. AMS has also been correlated with strain in rocks [*Borradaile*, 1991; *Parés et al.*, 1999; *Parés and Van der Pluijm*, 2003], and has been used to characterize soft-sediment deformation [*Schwehr and Tauxe*, 2003].

[6] Although magmatic dikes and injection clastic dikes are both related to hydrofracturing and fluid flow, they differ in several aspects. (1) The time of AMS acquisition of magmatic dikes may be very long due to the slow rate of mineral growth [*Féménias et al.*, 2004, and references therein]. On the other hand, because the magnetic minerals already exist, the origin AMS in clastic dikes is acquired rapidly, immediately after the emplacement process. (2) Natural fluidized sediments are characterized by turbulent flow in contrast to magma, which is more viscous [*Turcotte and Schubert*, 1982]. Little is known about the kinematics of the flowage of sediments within dikes during earthquakes, especially if the injected sediments are clay-rich. Nor is there much information about the acquisition of AMS fabric during sedi-

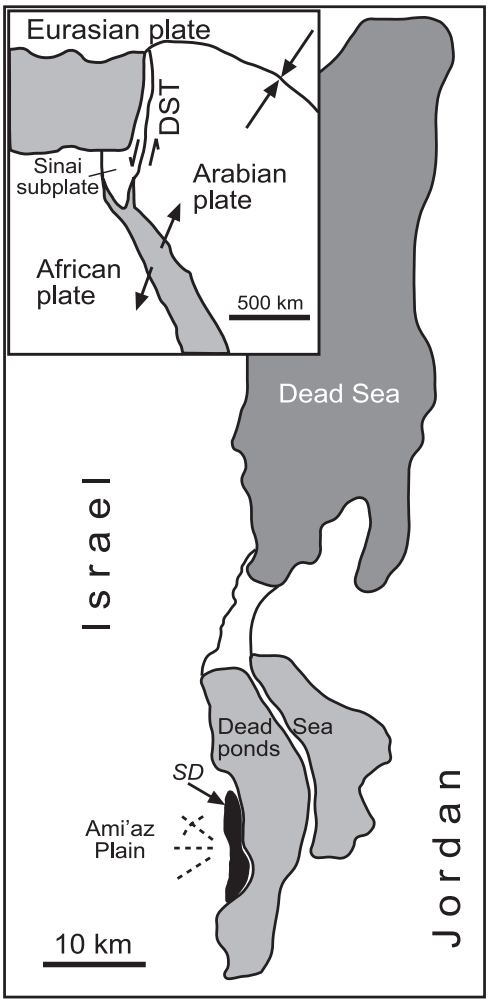

Figure 1. Location maps of the study area. The regional setting of the Dead Sea Transform (inset) and the Ami'az Plain with the clastic dikes marked schematically by broken lines. DST, Dead Sea Transform; SD, Sedom Diapir [after *Levi et al.*, 2006].

ment flow through a channel, especially under fast flow conditions.

[7] In a previous study [*Levi et al.*, 2006] we used the AMS fabric to distinguish between depositional and injection clastic dikes emplaced along the margins of the seismically active Dead Sea Transform. We showed that the AMS application provides a petrofabric tool to differentiate between clastic dikes of different origins [*Levi et al.*, 2006]. In the present study we use the AMS fabric to explore the emplacement mechanism and fluid flow of dozens of Holocene injection dikes that cross-cut late Pleistocene lacustrine soft rocks exposed in the southwestern margin of the Dead Sea basin. The results extend our knowledge on clastic transportation at fast flow, and improve the understanding of the clay-rich sediment fluidization process.

2. Geologic Setting

[8] The Ami'az Plain study area (Figure 1) is located west of the Mount Sedom salt diapir [*Zak*, 1967; *Weinberger et al.*, 2006a, 2006b] near the southwestern margin of the Dead Sea basin, along the segmented Dead Sea fault (transform) [e.g., *Quennell*, 1959; *Freund et al.*, 1968; *Garfunkel*, 1981]. The bedrock of the Ami'az Plain is the ~40 m thick Late Pleistocene lacustrine Lisan Formation consisting mostly of laminae of authigenic aragonite and gypsum layers alternating with fine detritus layers [*Begin et al.*, 1980]. A thin veneer of eolian and fluvial sediments covers large parts of the plain. The incision of Nahal (Wadi) Perazim in the Ami'az Plain exposed the entire Lisan section and about 250 clastic dikes, which are embedded within this section. The U-Th age of the Lisan Formation is between ~70,000 and 15,000 years B.P [*Haase-Schramm et al.*, 2004].

[9] The Dead Sea basin is a continental depression located within the rift valley that extends along the Dead Sea fault. The basin is bounded on the east and west by a series of oblique-normal step-faults. The Ami'az Plain is one of the downfaulted blocks developed within the rift valley. Paleoseismic records from the Dead Sea basin based on breccia layers reveal numerous $M > 5.5–6$ earthquake events during the last 70,000 years [e.g., *Marco and Agnon*, 1995; *Enzel et al.*, 2000; *Ken-Tor et al.*, 2001], as well as several $M > 7$ earthquake events [*Begin et al.*, 2005, and references therein]. Recent seismicity in the Dead Sea basin is presented by *Shapira* [1997]. The recorded strongest event in the Dead Sea basin was the $M = 6.2$ earthquake of 11 July 1927; its source mechanism was of a left-lateral motion [*Ben-Menahem et al.*, 1976; *Shapira et al.*, 1993].

[10] The injection dikes in the Ami'az Plain (Figure 2) are composed of green clay, silty quartz, and some aragonite fragments. These dikes, up to hundreds of meters long, 30 m high and up to 0.4 m wide, most probably originated in the lower layers of the Lisan Formation [*Levi et al.*, 2006]. They are arranged mainly in radial and tangential geometry. The connection of a green clay-rich layer of the Lisan Formation to the dike-fill observed in several dikes unequivocally indicates that they were formed by injection of material from the

Figure 2. (a) Clastic dike, filled with clay-rich sediment, cross-cutting the Lisan Formation about 12–18 m above its source layer. The dike branches upward into several strands (see arrows) which partly coalesce at different levels. (b) Two disconnected, partially overlapping dike segments in the upper section of the Lisan Formation. Similar to magmatic dikes [e.g., *Weinberger et al.*, 1995], this geometry hints at the role played by internal pressure during dike emplacement and horizontal transport of clastic material into the evolving dikes. Lisan laminae are not displaced along the dike walls, indicating that clastic dikes are extensional fractures. Note that because the dike segments are not physically connected to the surface, the flow within it had a lateral component.

clay-rich layer. The majority of dikes terminate against a 0.5-m-thick gypsum layer at the top of the Lisan section. The lower ends of the dikes are within alternating laminae of aragonite and gypsum layers of the lower Lisan Formation. At least five of these dikes are composed of several (up to 12) distinct vertical sheets of sediments, 0.02–0.05 m wide each, which we interpret as evidence of multiple injections. Occasionally, the injection dikes are wider in their lower part than in their upper part. Several injection dikes branch toward the surface and split into 3–5 large strands (Figure 2a) resembling dynamic fractures that bifurcate during upward propagation [e.g., *Bahat et al.*, 2004]. The large strands are typically segmented, forming numerous small-scale segments (~0.15 m height) about 13 m above the source layer. The architecture and discontinuity in the vertical section of these dike segments is compatible with a lateral propagation. The overlapping geometry between two segments implies opening of a fracture under internal pressure [e.g., *Delaney and Pollard*, 1981; *Weinberger et al.*, 1995] (see Figure 2b). *Levi et al.* [2006] concluded that the

formation of these dikes resulted due to seismic loading. Local vertical static pressure as a trigger is excluded mainly because the dike phenomenon is local and very close to the surface.

[11] Less common are depositional dikes composed of brownish silt, in places showing horizontal bedding planes, which resemble the veneer of surface sediments. These dikes always intersect the present surface and are commonly wider in their upper part.

3. AMS Application for Clastic Dikes

[12] AMS is a second-rank tensor which is described by its principal values and principal axes [*Borradaile and Jackson*, 2004, p. 300]. The principal values, τ_1, τ_2, and τ_3, correspond to the maximum, intermediate and minimum magnetic susceptibility magnitudes respectively, and the principal AMS axes are V_1, V_2 and V_3, respectively [*Tauxe*, 1998].

[13] In our previous study we showed that depositional dikes display a sedimentary AMS fabric in which V_3 axes are vertical and well grouped, whereas V_1 and V_2 axes are dispersed within the horizontal plane (Figure 3: A1). The values of the associated τ_1 and τ_2 are indistinguishable and characterized by oblate AMS ellipsoids [*Tarling and Hrouda*, 1993; *Borradaile and Henry*, 1997; *Liu et al.*, 2001]. The injection dikes, characterized by prolate or triaxial AMS ellipsoids, display a flow AMS fabric (Figure 3: B2–E2), suggesting that the flow direction is reflected by V_2 axes. In the present study, we elaborate various aspects of flow and flow fabric developed within injection dikes. We compare it with the AMS fabric that is formed by a viscous Newtonian flow in magmatic dikes, and with the flow fabric developed in low- to high-energy currents in sedimentary environments.

[14] In Newtonian flow, particle imbrication along the dike walls and prolate/triaxial AMS ellipsoids are expected [*Féménias et al.*, 2004, and references therein] (Figure 3: B1–B3). The imbrication helps to resolve the flow direction, with V_1 axes being the common flow indicator. In the dike core inverse fabric with oblate AMS ellipsoids are expected (Figure 3: B1.1, B2.1, and B3). In low-energy currents, particle imbrication results in slightly off-vertical V_3 axes [*Rees*, 1979] with oblate to very weak triaxial AMS ellipsoids (Figure 3: C1–C3). In moderate-energy currents, grain imbrication results in slightly off-vertical V_3 axes [*Tauxe*, 1998] and V_1 axes are inclined to the opposite flow direction (Figure 3: D1–D3). The flow directions may also be indicated by the inclinations of V_3 axes as well [*Rees and Woodall*, 1975; *Cagnoli and Tarling*, 1997; *Liu et al.*, 2001; and references therein]. In high-energy currents with particles entrained, V_1 axes are perpendicular to the flow direction and V_3 axes are commonly streaked, resulting in prolate or triaxial AMS ellipsoids [*Tauxe*, 1998, and references therein] (see Figure 3: E1–E3). In earthquake-induced injection dikes flow velocity is expected to be high, hence V_1 is expected to be perpendicular to the flow direction and streaked V_3–V_2 distributions may evolve (Figure 3: E1–E3). In the latter case, the flow direction would be indicated by either the V_2 or V_3 axes [*Tauxe*, 1998]. In both cases, the principal axes should be well grouped, characterizing a "flow fabric." Consequent deformation due to closure of pore space and expulsion of pore water contained in the sediment is not expected to modify the shapes of the AMS ellipsoids [*Parés et al.*, 1999].

4. Sampling Strategy and Methods

[15] A total of 312 samples were recovered from nine clastic dikes and country rocks. We carved 2.5-cm-cylinder pedestals using a sharp knife, and placed on them plastic araldite-glue-coated cylinders with no AMS signal. The dikes were sampled across their width and along their height, 8–35 specimens in each. On the basis of field observations, two of the dikes are depositional dikes (T and To) and seven are injection dikes (Tg, Tk, Tn, Tp, Q, Sb and TR). Twelve to twenty specimens were collected from two Lisan layers, one of which is the clay-rich source layer of Dike Q (Figure 4), and the other is an undisturbed layer.

[16] The sampling scheme of the seven injection dikes was as follows: Two dikes (Tg and Q) were sampled at different localities below the upper gypsum layer, along their height and length. An intensive sampling of Dike Q was carried out because it comprises several sheets (Qa, Qb, Qc, Qd; see Figure 4) that are connected to a Lisan source layer (SLQ). Dike TR is a multiple injection dike composed of 12 vertical bands of sediments. Three of these bands were sampled in several places along their heights. Dikelet Sb, one of the small-scale dikes extensively developed in the upper part of the Lisan section, was sampled along it length.

[17] Three dikes: Tk, Tp, and Tn, were sampled in the lower Lisan section near the level of the source layer (i.e., ~18 m below the upper gypsum layer). In each dike between 12 and 20 specimens were

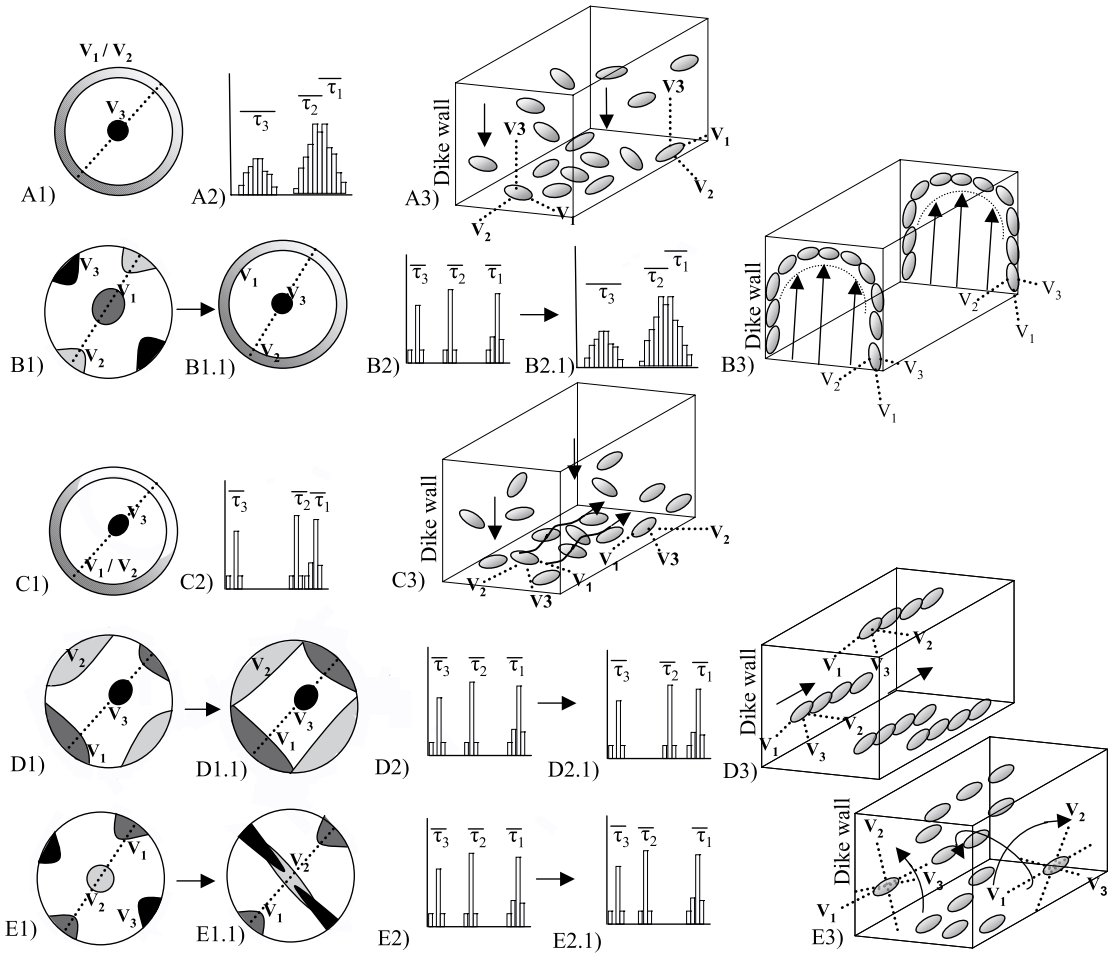

Figure 3. Anisotropy of magnetic susceptibility (AMS) for clastic dikes that were emplaced under different conditions. A1–E1: equal-area projections (lower hemisphere) of synthetic AMS principal axes and their confidence zones based on the bootstrap method: white region, distribution of V_1 axes; gray region, distribution of V_2 axes; black region, distribution of V_3 axes. Dike strike is marked by a dashed line. A2–E2: distribution of principal values (τ_1, τ_2, and τ_3) with 95% confidence bounds, using the bootstrap method [*Tauxe*, 1998]. A3–E3: Schematic illustration of various possibilities of particle distribution within clastic dikes. Arrows mark the direction of particle transportation. (A) Sedimentary (oblate) AMS fabric in depositional dikes. (B) Flow AMS fabric developed during injection of viscous Newtonian fluid and characterized by imbrications along the dike's walls. The flow direction is inferred on the basis of the imbrications of V_1 axes. The principal axes in the horizontal plane are either grouped, e.g., along the dike walls (B1), or dispersed, e.g., in the dike core (B1.1). The values of the AMS ellipsoids are either triaxial (B2) or oblate (B2.1). (C) Low-energy flow fabric of oblate to weak triaxial AMS ellipsoids. (D) Moderate-energy flow fabric of triaxial (D2) or weak triaxial (D2.1) AMS ellipsoids. The principal axes are either grouped in the horizontal plane (D1) or more dispersed (D1.1), depending on the flow rate. Interpretation of the flow direction is based on V_3 inclinations [e.g., *Liu et al.*, 2001] and is in opposite direction to V_1 axes inclinations [*Rees*, 1979; *Tauxe*, 1998]. (E) High-energy flow fabric of triaxial (E2) or weak triaxial (E2.1) AMS ellipsoids. The principal axes are either grouped (E1) or streaked (E1.1) due to rotation of particles during turbulent flow. V_1 axes might be orthogonal to the flow direction and either V_2 or V_3 axes indicate the flow direction.

evenly distributed across the dike width and between 5 and 9 specimens were sampled along the dike margins. This sampling strategy forms an "H-like shape" designed to detect possible particle imbrication and effect of syn- and post-shearing along the margins.

[18] The AMS was measured with a KLY-3S Kappabridge at the Geosciences Laboratory, University of Rennes 1, France. The principal susceptibility axes with the 95% confidence ellipses and the bootstrapped axes were analyzed with the program "programs magnetic anisotropy analysis"

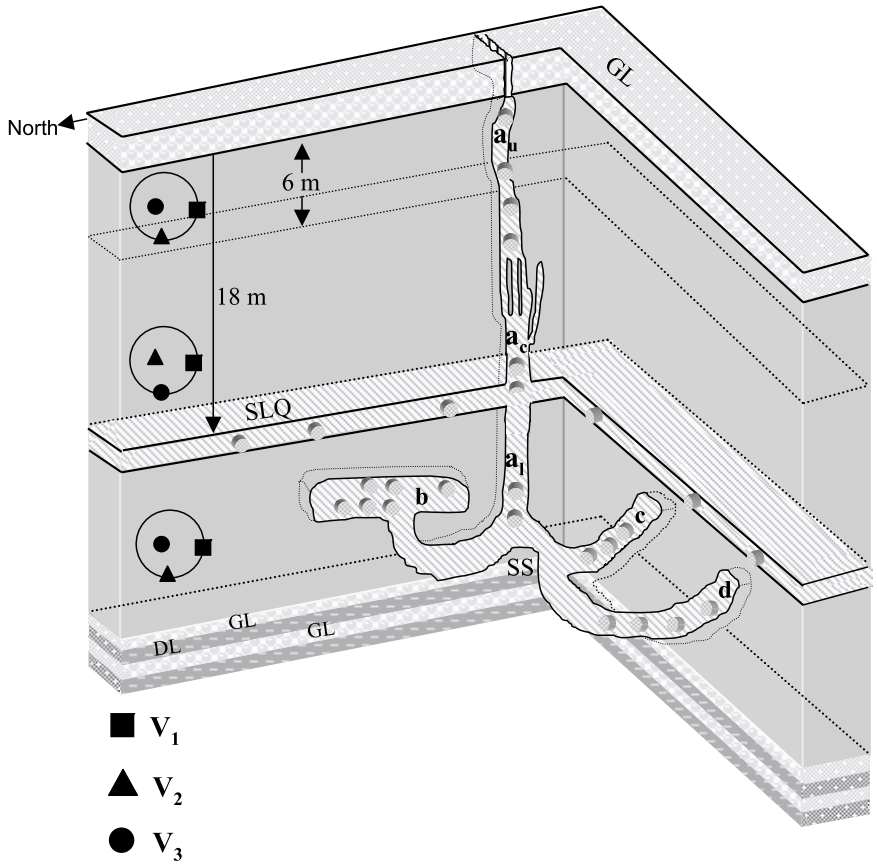

Figure 4. Schematic illustration of the Q dike system composed of the source layer Q (SLQ), Dike (a), and the sheets system (SS: b–d). The dike system is bounded below by a series of thin alternating gypsum layers (GL) and detritus (DL) and by a thick gypsum layer (GL) above. Cylinders mark sampling points and the stereograms showing schematic fabric variations along the dike height (see Figure 8).

written by Henry. B, Lienert. B, and Le Goff. M. The shapes of the AMS ellipsoids were also analyzed by the Bootstrapping method [*Tauxe*, 1998] PMAG software (L. Tauxe, 2002), assuming that the samples represent the whole population.

[19] Flow directions were analyzed following *Moreira et al.*'s [1999] procedure. To characterize the magnetic carriers of the dike's infill and the Lisan source sediments, we used 20 thermomagnetic curves and 20 hysteresis loops of specimens from the dikes.

5. Results

5.1. Rock Magnetism

[20] Thermomagnetic curves of green clay-rich sediments taken from the Lisan source sediments and dike infill exposed in the central and lower sections of the Lisan Formation show that the magnetic carrier is titanomagnetite (Figure 5a). Thermomagnetic curves of brownish clay-rich sediments taken from the dike infill exposed in the upper section of the Lisan Formation show that the magnetic carriers are titanomagnetite and maghemite (Figure 5b). The lack of hematite in the dike infill implies that oxidation played a minor role after its emplacement [*Aïfa and Lefort*, 2001].

[21] Hysteresis loops of clay-rich sediments taken from the Lisan source sediments and dike infill show that the ratio J_{rs}/J_r is near 0.1 and the H_{cr}/H_c is around 6.5 (Figure 5c). These values are strongly favored for multidomain (MD) grain size [*Day et al.*, 1977]. Comparison between the present results and published hysteresis loops of the Lisan sediments [*Marco et al.*, 1998] and clay sediments [e.g., *Schwehr and Tauxe*, 2003; *Cifelli et al.*, 2004] shows that the clay-rich sediments are of relatively large grain size.

[22] The mean magnetic susceptibility values ($K_{mean} = [k_1 + k_2 + k_3/3]$ [*Nagata*, 1961]) of all

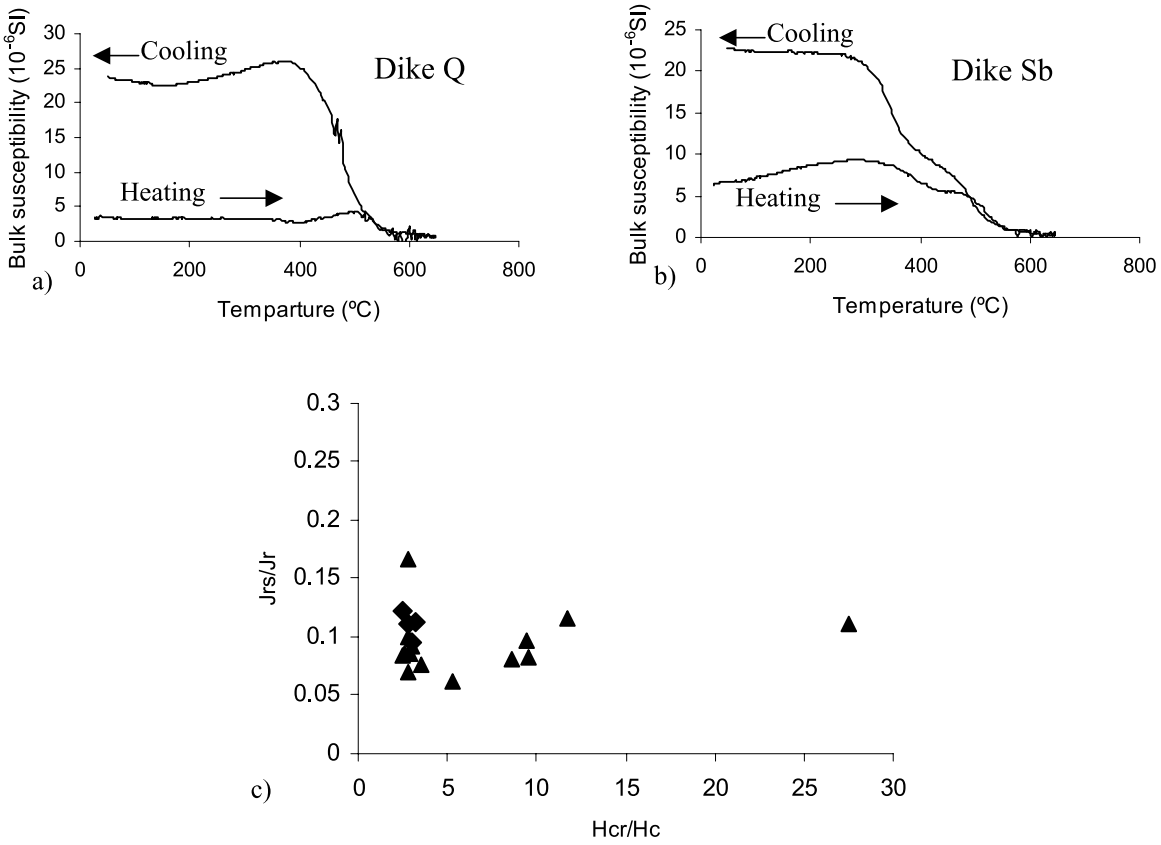

Figure 5. Rock magnetism of clastic dikes. (a) Representative thermomagnetic curve from Dike Q. The steep gradient of the susceptibility around 510°C is attributed to titanomagnetite [e.g., *Ferré et al.*, 2002]. (b) Thermomagnetic curve from Dike Sb. The inflection point around 350°C is attributed to maghemite [e.g., *Archanjo et al.*, 2000], and that around 510°C is attributed to titanomagnetite. (c) Day diagram [*Day et al.*, 1977] showing the results of 20 hysteresis loops of specimens from the margins and the centers of the dikes. Triangles, injection dikes; squares, depositional dikes. Jrs is the saturation remanence, and Jr is the saturation magnetization. Hcr is the coercivity of remanence, and Hc is the coercive force. The average ratio Jrs/Jr is near 0.1, and the average ratio Hcr/Hc is around ~6.5, suggesting multidomain grain size.

samples recorded from the clastic dikes and the Lisan source layer range between 40 and 360 $\times$ 10^{-6} SI. This range of values is typical for clay sediments [*Cifelli et al.*, 2004]. The average K_{mean} of the depositional dikes is ~225 $\times$ 10^{-6} SI whereas that of the injection dikes and their source layer is ~70 $\times$ 10^{-6} SI (Figure 6). This difference may reflect different sedimentary origins [e.g., *Liu et al.*, 2001]. The K_{mean} of all the sampled dikes decrease toward the bottom from 150 $\times$ 10^{-6} SI at the surface to 60 $\times$ 10^{-6} SI ~18 m below the upper gypsum layer (Figure 6).

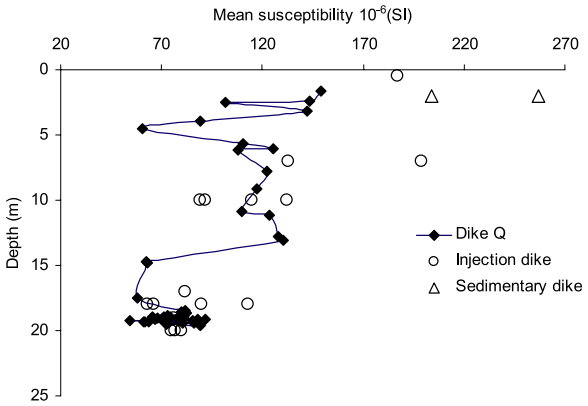

Figure 6. Variations of the mean susceptibility values with depth below the upper gypsum layer. Susceptibility values increase unmonotonously upward along Dike Q and all others dikes. Diamonds, Dike Q; circles, injection dikes; triangles, sedimentary dikes.

5.2. AMS

5.2.1. General

[23] The AMS fabrics of eight representative clastic dikes and the Lisan source layer are presented in Figures 7 and 8. The depositional dikes, repre-

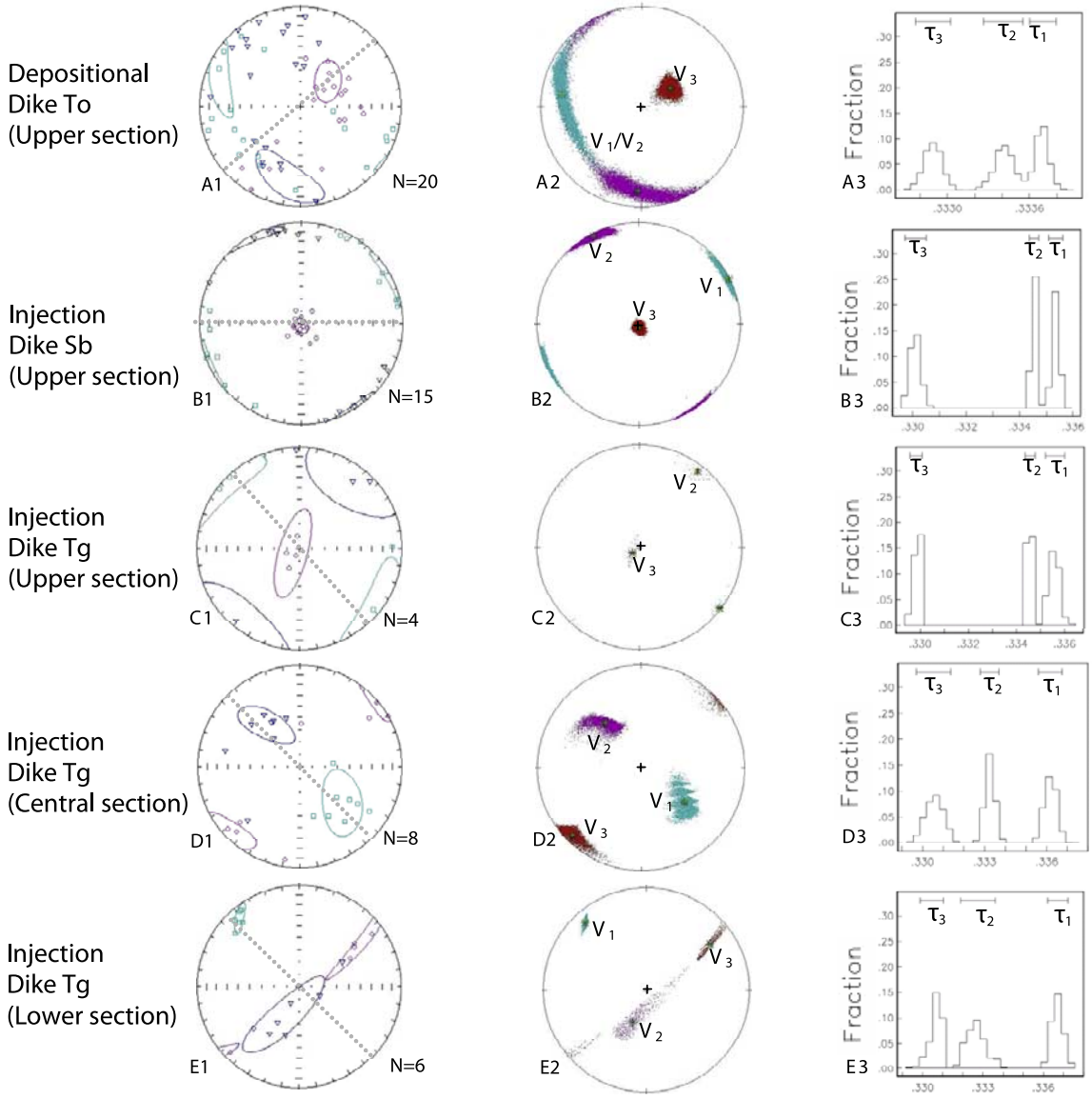

Figure 7. AMS of the depositional dike (Dike To, A) and six injection dikes (Dikes Sb, Tg, Tk, Tp, Tn, and TR). A1–J1: Lower-hemisphere, equal-area projections of AMS principal axes and the 95% confidence ellipses; squares represent V_1 axes, triangles represent V_2 axes, and circles represent V_3 axes. A2–J2: Lower-hemisphere, equal-area projections of AMS principal axes analyzed by the bootstrapping method. A3–J3: Principal values distribution with 95% confidence bounds. Dashed lines mark the dike strike. A2–A3 show a sedimentary fabric. B2–C2 and B3–C3 show grouped subvertical V_3 axes with weak triaxial flow fabric. D2–J2 and D3–J3 show subvertical V_2 axes with weak triaxial to triaxial flow fabric. Streaked V_2–V_3 fabric is seen in E2, G2, H2, I2, and J2. Notice that the 95% confidence ellipses look similar to the confidence zones analyzed by the bootstrap method (see also Figure 8).

sented here by Dike To (Figure 7: A), exhibit a sedimentary fabric (Figure 3: A) similar to that of the Lisan layer (Figure 8: A). This fabric also resembles that of a low velocity current (Figure 3: C).

[24] The injection dikes (Sb, Tg, Tk, Tp, Tn, TR) (Figure 7: B–J) and the Q system (Figure 8: B–F) have different and distinctive AMS fabrics. In these dikes the three principal axes are well grouped, whereas the V_2 axes are subvertical (Figure 7: D1–J1 and Figure 8: C1–E1) or subhorizontal (Figure 7: B–C and Figure 8: B–D, F) and the V_1 axes are subhorizontal, and parallel to the dike strike. In addition, the bootstrap statistics principal values

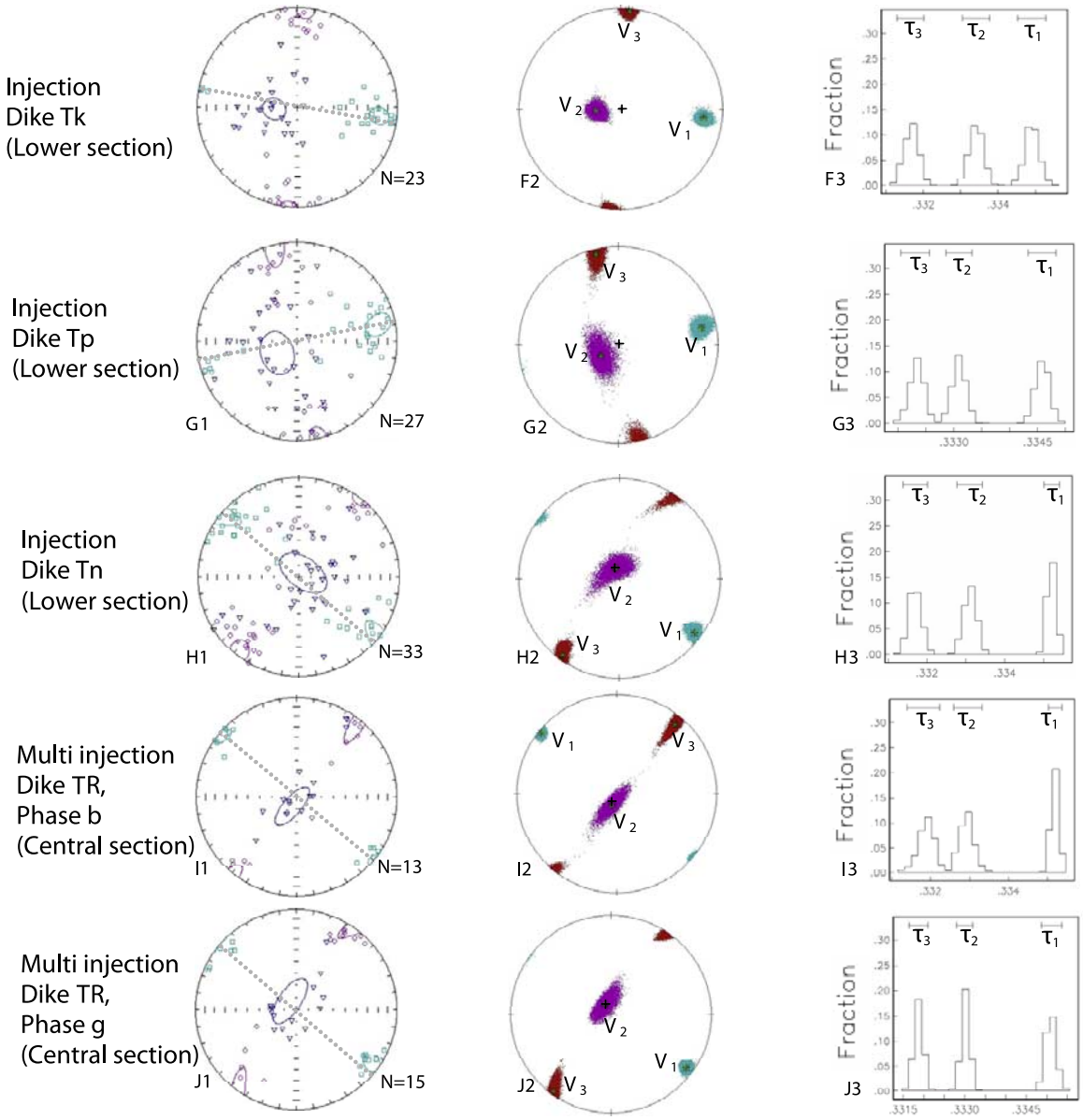

Figure 7. (continued)

define distinct triaxial AMS ellipsoids (Figure 7: B3–J3 and Figure 8: C3–F3).

5.2.2. Streaked AMS Pattern

[25] In the central-lower Lisan section the injection dikes are characterized by subhorizontally grouped V_1 axes, subvertical V_2 axes and a streaked AMS pattern (Figure 7: E2, G2, H2, I2, and J2 and Figure 8: E2). This pattern is usually composed of streaked V_2 and V_3 axes and, rarely, of V_2 and V_1 axes. It commonly consists of about 20% of the total projected principal axes. An analysis of principal values indicates that the AMS ellipsoids have a triaxial shape (Figure 9c) that is not formed by overlapping of the τ_2 and τ_3 principal values. The AMS analysis indicates that the streaked pattern is repeated and is dominant everywhere across the dike widths (Figures 9d and 9e).

5.2.3. Subvertical V_3 Axes

[26] In three dikes (Sb, Tg and Q) located between 0.1–6 and 18 m below the uppermost gypsum layer (Figure 7: B–C and Figure 8: C, D, and F) the three principal axes are well grouped, whereas the V_3 axes are subvertical. In these dikes weak triaxial to triaxial AMS ellipsoids were detected.

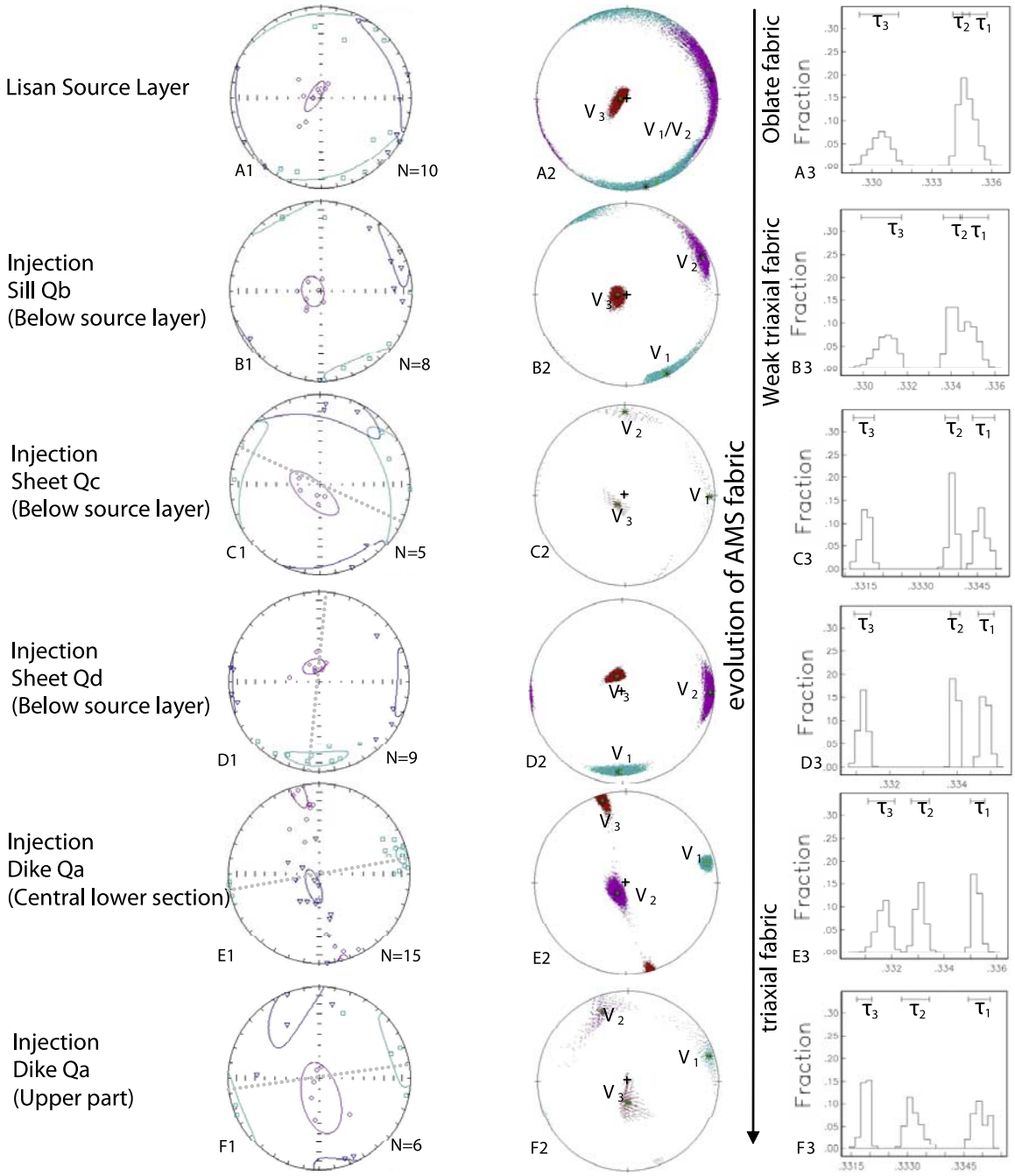

Figure 8. AMS of the Q dike system. For explanation of principal axes and values representation, see Figure 7. A: source layer; B–D: sheets Qb, Qc, Qd; E: Dike Qa, lower and central sections; F: Dike Qa, upper section. V_3 axes are subvertical in the lower and upper sections and subhorizontal in the central section. Evolution of AMS fabric from oblate to triaxial shape of the AMS ellipsoid is marked.

5.2.4. Q System

[27] The AMS results of the Q system show variations compatible with the location within the system (Figures 4 and 8). The Lisan source layer shows a sedimentary fabric with some inclination of the subvertical V_3 axes westward (Figure 9). Sheet Qb is characterized by well-grouped subvertical V_3 axes and subhorizontal V_1 and V_2 axes (Figure 8: B1 and B2). The latter directions are distinguishable along the horizontal plane and their principal values indicate oblate to weak triaxial

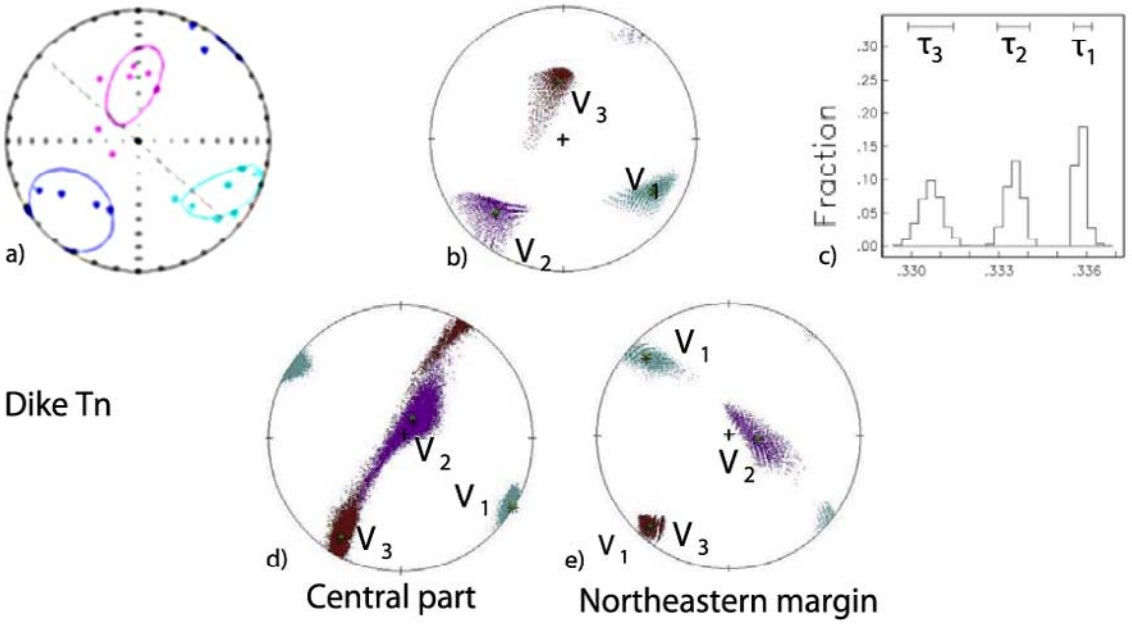

Figure 9. Analysis of streaked AMS pattern of Dike Tn. For explanation of principal axes and values representation, see Figure 7. (a)–(c) Streaked V_3 axes that are inclined more than 25° and their counterpart V_1 and V_2 axes. (d) and (e) Bootstrapped principal axes of the central part and northeastern margin of Dike Tn, respectively. Note that in a single dike the streaked AMS pattern changes from V_2–V_3 axes (Figure 9d) to V_2–V_1 axes (Figure 9e).

AMS ellipsoids. The inclined sheets Qc and Qd are also characterized by well-grouped subvertical V_3 axes, with weak triaxial AMS ellipsoids (Figure 8: C1–C3, D1–D3). On the basis of the similarity of these results to those presented in Figure 3 (C1–C2) and Figure 3 (D1–D2.1), the AMS fabrics in sheet Qb–Qd evolved during low to moderate velocity flow.

[28] Dike Qa is characterized by two different AMS fabrics, depending on their level in relation to the source layer and the uppermost gypsum layer as follows: (1) Between 6 m below the gypsum layer and 1 m below the source layer the dike is characterized by well-grouped subvertical V_2 axes and triaxial AMS ellipsoids (Figure 8: E1–E3). This AMS fabric is similar to that characterized in other dikes along the same interval of height (Figure 7: D–J). (2) From 12 m above the source layer up to the gypsum layer the dike is characterized by well-grouped subvertical V_3 axes and triaxial AMS ellipsoids (Figure 8: F1–F3). This AMS fabric is similar to that of Dike Sb (Figure 6: B1–B3) and Dike Tg (upper section, Figure 7: C1–C3).

[29] The shape of the AMS ellipsoid is defined by the T parameter [*Jelinek*, 1981] and varies from prolate, where $-1 \leq T \leq 0$, to oblate, where $0 \leq T \leq 1$. Figure 10a shows the variations of the T parameter in the source layer and Dike Qa. Away from Dike Qa, the source layer exhibits an oblate shape with an average value of $T \approx 0.6$. Close to the dike walls, the value of T decreases sharply below 0.6, and T reaches −0.35. The average T values of Dike Qa in the level of the source layer is −0.2, attesting to a prolate shape. While the T values of the source layer are distinguished from those of Dike Qa everywhere away from the dike, they overlap with the T values 0.6 m from each side of the dike walls (Figure 10b). These results imply that the source layer became fluidized at a distance on the order of ten times the dike width (∼0.06 m).

5.2.5. Orientation and P'-Parameter Value Variations Across the Dike Widths

[30] The bootstrap analysis across the width of Dikes Tk, Tp, and Tn reveals that the overall shape of the AMS ellipsoids varies between triaxial to weak triaxial.

[31] Comparing the three principal axes in these three dikes reveals that the orientations of the V_2 axes vary, and the orientations of the V_1 and V_3

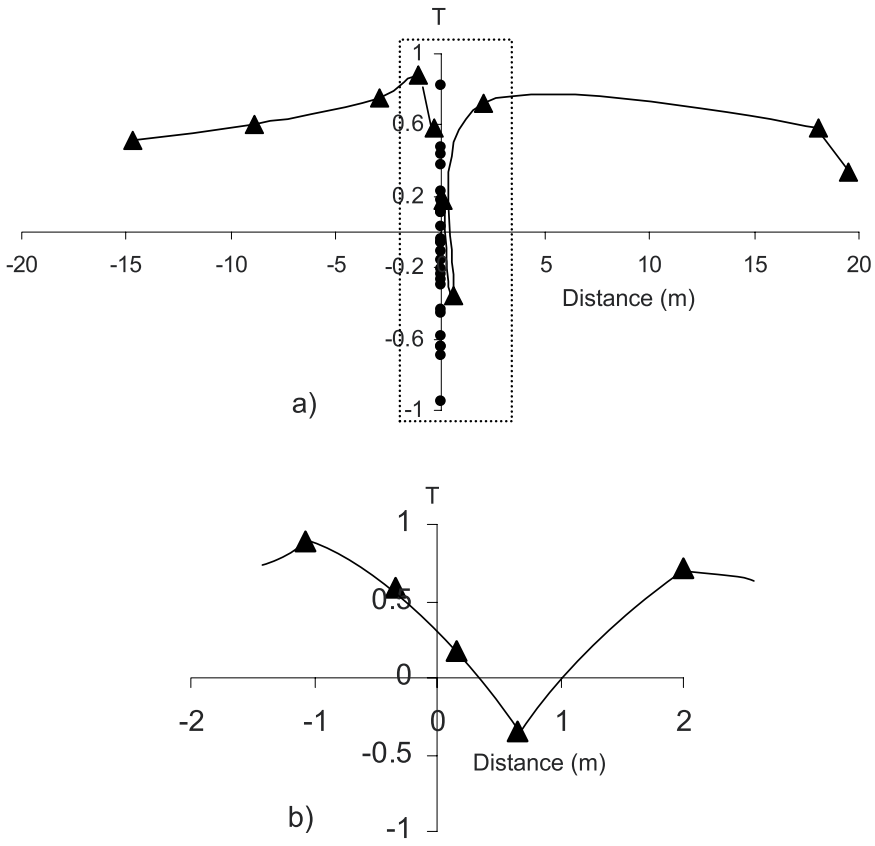

Figure 10. Variations of T-parameter (T) values in the Q system with respect to the distance from the dike centerline. Triangles, source layer; circles, Dike Qa. The marked area in Figure 10a is enlarged in Figure 10b.

axes are stable. For example, the V_2 orientations in Dike Tp are spread over a sector of 100°, whereas those of the V_1 and V_3 axes are within only 10° and 20°, respectively (Figure 11a).

[32] Variations of the P' parameter (the corrected anisotropy degree [*Jelinek*, 1981]) may be attributed to shear strain variations along the dike width during flow [*Féménias et al.*, 2004, and references therein]. Generally, the P' parameter is characterized by a peak value around the dike centers. Figure 11b shows that the variations in values of the P' parameter across Dike Tp resemble two semicircles, which seem to coincide with the wavy-like variations of the V_2 orientations across Dike Tp.

5.2.6. Orientation of Flow Directions

[33] We analyzed the absolute flow direction and possible imbrications in Dikes Tk, Tp, and Tn, following *Moreira et al.*'s [1999] procedure. These dikes were sampled more intensively along their borders and hence are suitable for this analysis. The analysis of the three dikes indicates that (1) the V_1–V_2 planes are inclined downward and (2) the mean directions are not statistically significant (Figure 12a). Hence it is most likely that the inclined planes show pseudo-imbrications along the dike walls, implying a downward flow direction (Figure 12b). We examined the possibility of imbrications by analyzing also the V_1–V_3 and V_2–V_3 planes but found no imbrications in these planes.

6. Discussion

6.1. Rock Magnetism

[34] The main magnetic carriers of the green clay-rich sediments from the Lisan source sediments and dike infill, based on thermomagnetic curves and hysteresis loops, are multidomain grains of titanomagnetite (Figure 5). The state of the titanomagnetite domain might play an important role in

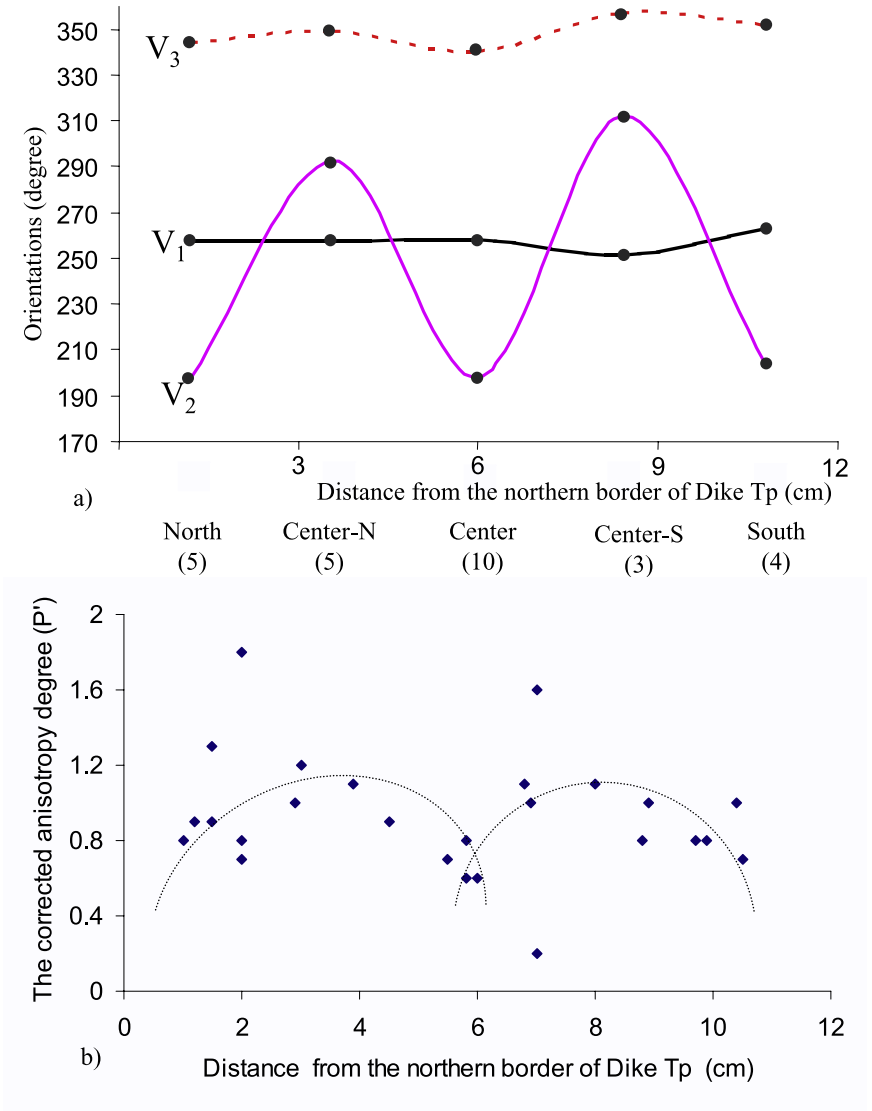

Figure 11. (a) Variations of V_1, V_2, and V_3 orientations across Dike Tp. The orientations are based on the bootstrapped AMS principal axes in lower hemisphere. Dike width is divided into five zones for which the averaged bootstrapped orientations were analyzed separately. Number of analyzed samples is indicated below each zone. V_1 and V_3 have stable orientations, while those of V_2 are scattered. (b) Variations of the P' parameter values across Dike Tp. Semicircles with peaks at ~3.5 cm from the dike's walls show possible pattern of value variations.

the acquisition of AMS fabrics. For multidomain grains the magnetization has maximum values in the direction of the grain's long axis ("normal" fabric), while in single-domain grains an "inverse" fabric with maximum susceptibility in the direction of the grain's short axis may occur [*de Wall et al.*, 2004, and references therein]. The parameters of the hysteresis loops are strongly related to multidomain grains; hence "normal" AMS fabrics are expected, and there is no correlation between grain size and sampling location along the Lisan section. Moreover, the increase of the mean susceptibility values upward, toward the surface (Figure 6), and the addition of maghemite as a magnetic carrier are not correlative to variations of magnetic fabrics along the dike high. The lack of increasing mean susceptibility values toward the bottom indicates that it was not affected by compaction. In Dike Q, similar AMS fabric was detected in the sheet system above the lower gypsum layer and in the upper part below the upper gypsum layers, although the mean susceptibility values vary significantly between these parts. Hence it is likely that magnetic-fabric variations are associated with var-

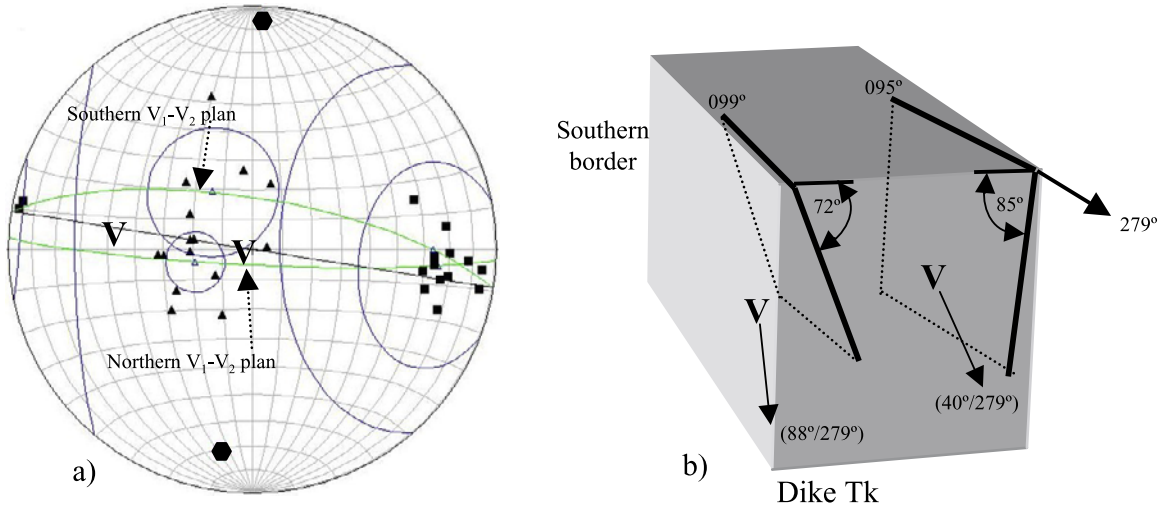

Figure 12. Analysis of the flow directions in Dike Tk, following *Moreira et al.*'s [1999] procedure. (a) Lower-hemisphere, equal-area projections of V_1-V_2 planes. Principal axes V_1 and V_2 are marked by squares and triangles, respectively; the ellipses are 95% confidence ellipse. Each plane is projected by the two mean vectors. Diamonds represent poles to the planes, and the solid line represents the dike strike. The flow vector V is found by taking 90° backward to the stereogram center from the intersection point between those planes and dike strike. Generally, the mean vectors are associated with large 95% confidence ellipses, but with downward flow direction. (b) Schematic illustration of V_1-V_2 planes along the borders of Dike Tk.

iations in the flow regime and not with "inverse" fabric, compaction or alteration effects.

6.2. Triaxial AMS Shape in Clastic Dikes

[35] The depositional dikes in the Ami'az Plain are characterized by sedimentary oblate AMS ellipsoids, whereas the injection dikes are characterized by distinct triaxial AMS ellipsoids. We interpret the latter AMS fabric as evidence that the clastic material within the injection dikes was emplaced by flow. We suggest that the detected AMS fabric provides several constraints on the emplacement mechanism and fluid flow of injection dikes. The abundance of triaxial AMS ellipsoids supports injection of clastic material simultaneously with fracturing or with the opening of existing clamped fractures in the Lisan host rock. This is because dynamic fracturing is favored for upward propagation and triaxial AMS ellipsoids were detected along the dike widths as well. The simultaneous fracturing and injection of clastic material up to the surface prevented deposition of clastic materials from above and the collapse of the weak and friable fissure walls. If the fissures were open for some time, then sedimentary fabric should have developed within the dikes; but such a fabric was not found, even in dikes that were intensively sampled (e.g., Dike Tk).

[36] Flow of the clay-rich sediment from the source layer into the evolving injection dikes has been referred to as fluidization [*Levi et al.*, 2006]. The variations of the T parameter in the source layer indicate that the fluidization process formed closed to the dike emplacement. The preservation of AMS flow fabric within the dikes suggests that the water content involved in the fluidization process was relatively low; otherwise suspended particles might have produced a sedimentary AMS fabric immediately after the injection. Low water content is not compatible with the sand liquefaction process, which seems to be associated with more water than the fluidization. In the sand liquefaction process much water is moved from the saturated layer upward because, comparing to the suggested fluidization, it is associated with an extensive layer that underwent liquefaction. Recently, *Heifetz et al.* [2005] suggest that liquefaction in soft sediment may occur immediately after the main shock by shear that induces Kelvin-Helmholtz instability. *Bachrach et al.* [2001] suggest that liquefaction in soft sediment is a direct result of the shock waves, compatible with loading by P wave, without the need of an indirect shear displacement mechanism and induced porosity reduction.

6.3. Moderate-Energy Flow Fabric

[37] In several dikes the triaxial AMS ellipsoids are associated with well-grouped subvertical V_3 axes

and well-grouped subhorizontal V_1 and V_2 axes. This fabric indicates lateral transport of clastic material (i.e., horizontal flow; Figure 3: D). This type of AMS fabric is found in dikes and sheets that were emplaced in the section between the lower and the upper gypsum layers. Hence the gypsum layers served as mechanical boundaries for vertically propagating fractures and caused horizontal flow of the fluidized clastic material. Horizontal flow is also in agreement with field observations that show vertical discontinuity between dike segments and between them and the surface (e.g., Dikelet Sb, Figures 2b and 7 (B)). A similar fabric was also documented in magmas [*Cagnoli and Tarling*, 1997; *Baer et al.*, 1997; *Abelson et al.*, 2001] and sediments [*Rees and Woodall*, 1975; *Rees*, 1979; *Tauxe*, 1998; *Liu et al.*, 2001] and interpreted as an indication for horizontal flow as well.

6.4. High-Energy Flow Fabric

6.4.1. Streaked AMS Fabric

[38] Streaked AMS patterns that were found in many injection dikes (Figures 7–9) are repeated everywhere along the dike widths. *Tarling and Hrouda* [1993, pp. 105–106] and *Tauxe* [1998, pp. 231–232] described the streaked AMS pattern in sediment flow and suggested that it resulted from particles that were entrained under conditions of high-energy current flow, that V_1 axes are perpendicular to the flow direction, and that in such a case, either V_2 or V_3 axes indicate the flow direction. This flow fabric indicates that during high-energy flow, rotation of particles is parallel either to V_2–V_3 planes or to V_2–V_1 planes, most likely due to local turbulence. Our analysis shows that for each dike about 80% of the V_2 axes are subvertical and 20% are streaked toward the horizontal plane. The latter axes seem to represent local eddies and swirls.

[39] Two types of streaked AMS patterns are detected: (1) streaked V_3–V_2 distributions and (2) streaked V_2–V_1 distributions. The former pattern is by far more abundant. The two types of streaked AMS patterns imply two types of subvertical currents, which differ in the way particles are entrained in them. Rotation of particles from a vertical direction is attributed to small eddies that were generated by the high-energy turbulent flow. The final effect of these eddies is locked particles at opposite directions to the main flow direction as detected in V_2 orientations (see below), and a P' parameter across the dike width (Figure 11). Variations of the P' parameter are related to shear strain variations [*Féménias et al.*, 2004]. Therefore we suggest that in several dikes (e.g., Dike Tp, Figure 11b), where the P' parameter along the width of a dike is not uniform, one or two symmetrical local eddies coexisted during clastic transport. This possibility adequately explains the rotated orientations of several V_2 axes around a vertical axis.

6.4.2. Subvertical V_2 Axes as Indicators for Fast Flow

[40] Several studies of magmatic dikes suggest that V_2 axes can indicate the flow direction [e.g., *Moreira et al.*, 1999; *Geoffroy et al.*, 2002; *Lefort et al.*, 2006], but this is yet not well established [*Callot et al.*, 2001] and not well understood [*Cañón-Tapia*, 2004]. *Tarling and Hrouda* [1993, pp. 100–101] suggested that in high-energy currents (>cm/s), elongated grains roll their long axes perpendicular to the flow direction.

[41] Turbulence flow effect, reverse fabric, hydrothermal alteration, and post tectonic activities were suggested to explain why in some cases the V_2 axes are parallel to the flow direction [*Cañón-Tapia*, 2004, pp. 213–214, and references therein]. On the basis of the following arguments, we suggest that subvertical V_2 axes can serve as flow indicators for clastic dikes in high velocity conditions (Figure 3: E). First, the expected dominant flow in several dikes which were sampled above their source layer (e.g., Dike Q, Dike Tk, Dike Tp and Dike Tn) is vertical, and the V_2 axes in these samples is vertical too. Second, in the lower and upper parts, near the gypsum layers, where horizontal flow in the dikes is more plausible, the V_3 axes are subvertical. If indeed horizontal flow was dominant in the central part of the section too, the magnetic fabric should be consistent with subvertical V_3 and not subvertical V_2 axes. There are no indications for reverse fabric or hydrothermal alteration or post tectonic activities and they cannot be satisfactorily explained. Therefore the most reasonable explanation is that the subvertical flow, indicated by the V_2 axes, is dominant in the central segment. Third, the V_2 axes are the common axes in the two coexisting streaked V_1–V_2 and V_2–V_3 AMS patterns (see above), implying that the particles are rotated in the vertical planes. This may be explained only by a dominance of the subvertical flow direction because in a turbulence flow regime, the main flow is most likely to generate an anti-eddy flow direction in the flow planes [*Baer et al.*,

1997]. Fourth, streamlines determine the direction of the flow indicator axes, whereas the other two axes are "passive" and range in a plane vertical to this indicator. During flow, mainly in the turbulence flow regime, the streamlines are not always parallel to each other. Therefore it is most likely that even small modifications of streamlines will be expressed by variations of the "active marker" orientations. The variations in V_2 orientations and the stabilization of V_1 and V_3 axes suggest that the V_2 axes are the flow indicators. This suggestion is also strengthened by the similar profile value variations of the P' parameter across the dike widths (see below). On the basis of the above four arguments we suggest that the V_2 axes represent the flow indicators for the streaked AMS fabric detected in the clastic dikes.

[42] We further presume that the horizontal pressure gradient that caused the horizontal flow was lower than the vertical one, because the latter was affected by the overburden. Hence it is likely that the lateral transport of clastic material occurred under lower energy than that of the vertical transport of clastics. This is in agreement with the detected moderate-energy flow fabric described above (Figure 3: D).

6.4.3. Imbrications Along the Dike Walls

[43] Following *Moreira et al.*'s [1999] procedure, we found that the V_1–V_2 planes show pseudo-imbrications along the dike walls, and the mean directions are not statistically significant (Figures 12a and 12b). The trends of the pseudo-imbrications imply a downward flow direction toward the source layer, which is not plausible. It seems that these pseudo-imbrications formed due to local eddies similar to what *Baer et al.* [1997] described for turbulent pyroclastic flow. Pseudo-imbrications might also be the result of gravity effects at the final stage of fluidization. However, both effects seem to be local and are not related to imbrications that evolve during simple Newtonian flow [*Féménias et al.*, 2004, and references therein].

6.4.4. Viscous Flow in High Shear Strain Regimes

[44] Theoretically, channel laminar flow of Newtonian fluid is associated with strain variations across the dike width [e.g., *Correa-Gomes et al.*, 2001] that may change the AMS fabric accordingly. Adjacent to the margins the particles may imbricate, whereas the V_1 axes will be subparallel to the dike plane. In the central part of the dike the values of the P' parameter may be relatively lower due to the oblate AMS shape [e.g., *Correa-Gomes et al.*, 2001].

[45] The transition from oblate fabrics in the dike center to triaxial fabric may depend on the shear strain rate and fluid properties [*Paterson et al.*, 1998; *Féménias et al.*, 2004].

[46] In channel flow of non-Newtonian fluid (power-flow fluid), the magnetic fabric is expected to be constant along most of the dike width and V_1 axes are parallel to the dike walls [*Féménias et al.*, 2004, and references therein]. Because significant velocity gradients exist only very close to the dike walls, imbrications are restricted to very close proximity to the dike borders.

[47] *Paterson et al. [1998*, and references therein] suggested that a linear prolate fabric forms parallel to the flow direction in acceleration zones under high strain conditions and an oblate fabric develops at high angles to flow directions under lower strain conditions. Recent experiments by *Kratinová et al.* [2006] show that in low velocity zones oblate fabrics with imbrications along the walls formed, whereas in convergent flows where flow rates are higher and the strain rate increases, prolate fabrics parallel to the flow directions develop.

[48] The transition from Newtonian to non-Newtonian fluids may be associated with an increase in fluid internal cohesion accompanied by an increase in particle transport, blocking effects and mechanical interactions between particles in the same direction [*Correa-Gomes et al.*, 2001; *Sanin*, 2002]. On the other hand, *Arbaret and Diot* [1996] show that in low concentrated suspension, under large shear strains the orientation of the long axis of the particles tends to remain subparallel to the shear plane. That means that even in fluids, which are considered to behave more like Newtonian fluid, the particles' position may change depending on the shear rate condition.

[49] In the present study triaxial to weak triaxial AMS shapes are evident and persist across the dike widths, and the imbrications of the V_1–V_2 planes along the dike walls are insignificant. Also, the values of the P' parameter generally do not decrease toward the central part of the clastic dikes. Hence, on the basis of the AMS results, we suggest that the fluidization of the clay-rich sediment and flow of the clastic material was mainly associated with high-energy flow and high shear rate.

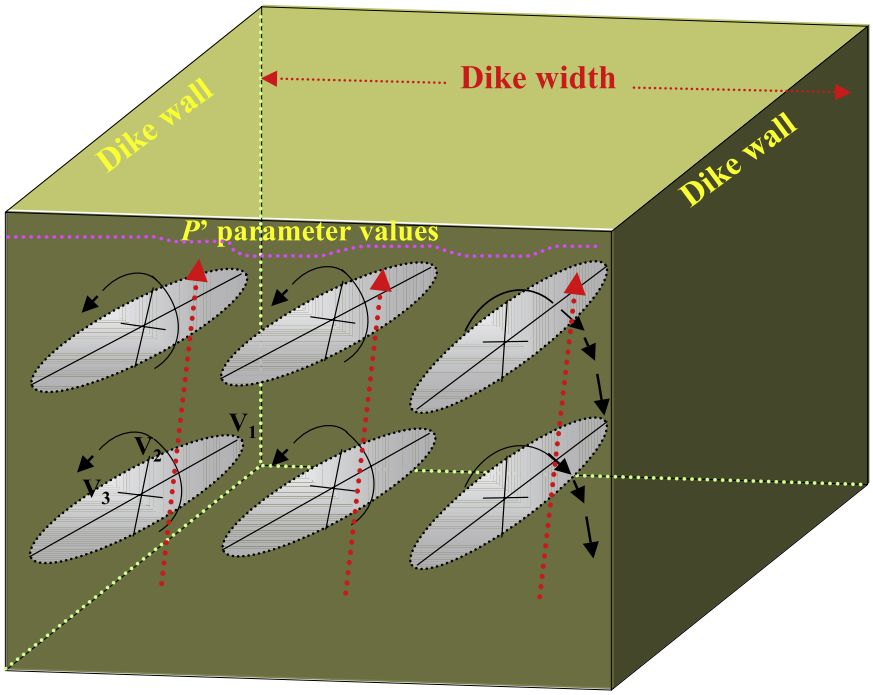

Figure 13. Schematic illustration showing the alignment of elongated grains in an injection dike during high-energy flow. Dashed red arrows indicate the main flow direction, and solid black arrows show the local directions of grain rotation. Dashed pink line indicates schematically the P' parameter values across the dike width. Due to local eddies, small modification of the P' values may occur. The overall flow direction is vertical, parallel to the intermediate axes of the grains, which are corresponding to V_2 axes. Note that in reality dike length is tens of times longer than the dike width.

[50] The proximity of the dikes to an active plate boundary makes earthquakes the most plausible trigger for fluidization. Paleoseismic studies indicate that many M > 6 earthquakes occurred during the last 15,000 years along the Dead Sea fault zone [e.g., *Begin et al.*, 2005, and references therein]. The AMS analysis and field observations clearly demonstrate that the formation of most clastic dikes in the Ami'az Plain are associated with fluidization triggered by strong earthquakes along the Dead Sea Transform after the deposition of the Lisan Formation, i.e., post 15 ka.

7. Summary

[51] Exploring the clastic dikes in the Ami'az Plain by using the AMS method leads to the following conclusions:

[52] 1. Fracturing and fluidization could have occurred either simultaneously or fracturing occurred prior to injection. Distinguishing between the two processes is not simple in magmatic dikes, and certainly not in clastic dikes. On the basis of the dynamic fracture pattern, we tend to accept that both fracturing and fluidization occurred simultaneously. Hence, during the fracturing process the inner pressure gradient was also involved in opening the fracture walls. This conclusion fits the intuitive idea that clastic dikes are structures that develop in a hydrofracturing process.

[53] 2. The flow kinematics manifested in the last stage of the clastic dike development reveals that the flow was fast due to a high pressure gradient and local turbulences were generated. This gradient also generated dynamic fractures that propagated in the front of the main dike channels. A high shear rate along the dike widths due to fast flow resulted in magnetic fabrics which are aligned like in non-Newtonian flow. We assume that the change of the magnetic fabric from a "normal case," where V_1 axes are parallel to the flow direction, to an "abnormal case" due to turbulent flow, may be one of the main explanations for the inverse fabric phenomena, and should be taken into consideration in the future (Figure 13).

[54] 3. Fluidization of clay-rich sediment may form in a different mechanism than that of the known

sand liquefaction process. Assuming that the fluidization process may develop by compression compatible with P waves during an earthquake event implies that porosity reduction is not necessary as in liquefaction mechanism. Therefore fluidization mechanism of clay-reach sediment should be taken into account when considering earthquake hazards.

Acknowledgments

[55] This study was supported by grants from the Israeli Ministry of National Infrastructures and the Arc en Ciel – Keshet program, French and Israeli ministries of science. We thank John Tarduno, the editor of G-Cubed, and we are indebted to Graham Borradaile and an anonymous reviewer for providing constructive and very helpful reviews. Tsafrir Levi thanks Moshe Arnon and Yaacov Rafael for their help in the field during the hot days at the Dead Sea.

References

Abelson, M., G. Baer, and A. Agnon (2001), Evidence from gabbro of Troodos ophiolite for lateral magma transport along a slow-spreading mid-ocean ridge, *Nature*, *409*, 72–75.

Aïfa, T., and J. P. Lefort (2001), Relationship between dip and magma flow in the Saint-Malo dolerite dyke swarm (Brittany, France), *Tectonophysics*, *331*, 169–180.

Arbaret, L., and H. Diot (1996), Shape fabrics of particles in low concentration suspensions: 2D analogue experiments and application to tiling in magma, *J. Struct. Geol.*, *18*(7), 941–950.

Archanjo, C. J., R. I. Trindade, J. W. P. Macedo, and M. G. Araújo (2000), Magnetic fabric of a basaltic dyke swarm associated with Mesozoic rifting in northeastern Brazil, *J. S. Am. Earth Sci.*, *13*, 179–189.

Bachrach, R., A. Nur, and A. Agnon (2001), Liquefaction and dynamic poroelasticity in soft sediments, *J. Geophys. Res.*, *106*(B7), 13,515–13,526.

Baer, E. M., R. V. Fisher, M. Fuller, and G. Valentine (1997), Turbulent transport and deposition of the Ito pyroclastic flow: Determinations using anisotropy of magnetic susceptibility, *J. Geophys. Res.*, *102*(B10), 22,565–22,586.

Baer, G. (1995), Fracture propagation and magma flow in segmented dykes: Field evidence and fabric analyses, Makhtesh Ramon, Israel, in *Physics and Chemistry of Dykes*, edited by G. Baer and A. Heimann, pp. 125–140, A. A. Balkema, Brookfield, Vt.

Bahat, D., A. Rabinovitch, and V. Frid (2004), *Tensile Fracturing in Rocks*, 557 pp., Springer, New York.

Begin, Z. B., Y. Nathan, and A. Ehrlich (1980), Stratigraphy and facies distribution in the Lisan Formation—New evidence from the area south of the Dead Sea, Israel, *Isr. J. Earth Sci.*, *29*, 182–189.

Begin, Z. B., D. M. Steinberg, G. I. Ichinose, and S. Marco (2005), A 40,000 year unchanging seismic regime in the Dead Sea rift, *Geology*, *33*(4), 257–260.

Ben-Menahem, A., A. Nur, and M. Vered (1976), Tectonics, seismicity and structure of the Afro-Eurasian junction—The breaking of an incoherent plate, *Phys. Earth Planet. Inter.*, *12*, 1–50.

Borradaile, G. J. (1991), Correlation of strain with anisotropy of magnetic susceptibility (AMS), *Pure Appl. Geophys.*, *135*, 15–29.

Borradaile, G. J., and B. Henry (1997), Tectonic applications of magnetic susceptibility and its anisotropy, *Earth Sci. Rev.*, *42*, 49–93.

Borradaile, G. J., and M. Jackson (2004), Anisotropy of magnetic susceptibility (AMS): Magnetic petrofabrics of deformed rocks, in *Magnetic Fabric Methods and Applications*, edited by F. Martin-Hernández et al., *Geol. Soc. Spec. Publ.*, *238*, 299–360.

Cagnoli, B., and D. H. Tarling (1997), The reliability of anisotropy of magnetic susceptibility (AMS) data as flow direction indicators in friable base surge and ignimbrite deposits: Italian examples, *J. Volcanol. Geotherm. Res.*, *75*, 309–320.

Callot, J. P., L. Geoffroy, C. Auboug, J. P. Pozzi, and D. Mege (2001), Magma flow directions of shallow dykes from the East Greenland volcanic margin inferred from magnetic fabric studies, *Tectonophysics*, *335*, 313–329.

Cañón-Tapia, E. (2004), Anisotropy of magnetic susceptibility of lava flows and dykes: A historical account, in *Magnetic Fabric Methods and Applications*, edited by F. Martin-Hernández et al., *Geol. Soc. Spec. Publ.*, *238*, 205–225.

Cifelli, F., F. Rossetti, M. Mattei, and A. M. Hirt (2004), An AMS, structural and paleomagnetic study of Quaternary deformation in eastern Sicily, *J. Struct. Geol.*, *26*, 29–46.

Correa-Gomes, L. C., C. R. Souza Filho, C. J. F. N. Martin, and E. P. Oliveira (2001), Development of symmetrical and asymmetrical fabrics in sheet-like igneous bodies: The role of magma flow and wall-rock displacements in theoretical and natural cases, *J. Struct. Geol.*, *23*, 1415–1428.

Day, R., M. D. Fuller, and V. A. Schmidt (1977), Hysteresis properties of titanomagnetites: Grain size and compositional differences, *Phys. Earth Planet. Inter.*, *13*, 260–267.

de Wall, H. D., A. Kontny, and C. Vahle (2004), Magnetic susceptibility zonation of the melilititic Riedheim dyke (Hegau volcanic field, Germany): Evidence for multiple magma pulses?, *J. Volcanol. Geotherm. Res.*, *131*, 143–163.

Delaney, P. T., and D. D. Pollard (1981), Deformation of host rocks and flow of magma during growth of Mintette dikes and breccia-bearing intrusions near Ship Rock, New Mexico: U.S. Geol. Surv. Prof. Pap., *1202*, 1–61.

Enzel, Y., G. Kadan, and Y. Eyal (2000), Holocene earthquakes inferred from a fan-delta sequence in the Dead Sea graben, *Quat. Res.*, *53*, 34–48.

Féménias, O., H. Diot, T. Berza, A. Gauffriau, and D. Demaiffe (2004), Asymmetrical to symmetrical magnetic fabric of dikes: Paleo-flow orientations and paleo-stresses recorded on feeder-bodies from the Motru Dike Swarm (Romania), *J. Struct. Geol.*, *26*, 1401–1418.

Ferré, E. C., C. Bordarier, and J. S. Marsh (2002), Magma flow inferred from AMS fabrics in a layered mafic sill, Insizwa, South Africa, *Tectonophysics*, *354*, 1–23.

Freund, R., I. Zak, and Z. Garfunkel (1968), Age and rate of sinistral movement along the Dead Sea Rift, *Nature*, *220*, 253–255.

Galli, P. (2000), New empirical relationships between magnitude and distance for liquefaction, *Tectonophysics*, *324*, 169–187.

Garfunkel, Z. (1981), Internal structure of the Dead Sea leaky transform in relation to plate kinematics, *Tectonophysics*, *80*, 81–108.

Geoffroy, L., J. P. Callot, C. Aubourg, and M. Moreira (2002), Magnetic and plagioclase linear fabric discrepancy in dikes: A new way to define the flow vector using magnetic foliation, *Terra Nova*, *183*, 183–190.

Haase-Schramm, A., S. L. Goldstein, and M. Stein (2004), U-Th dating of Lake Lisan aragonite (late Pleistocene Dead Sea) and implications for glacial East Mediterranean climate change, *Geochim. Cosmochim. Acta*, *68*, 985–1005.

Heifetz, E., A. Agnon, and S. Marco (2005), Soft sediment deformation by Kelvin Helmoltz Instability: A case from Dead Sea earthquakes, *Earth Planet. Sci. Lett.*, *236*, 497–504.

Jelinek, V. (1981), Characterization of magnetic fabric of rocks, *Tectonophysics*, *79*, 63–67.

Ken-Tor, R., A. Agnon, Y. Enzel, M. Stein, S. Marco, and J. F. W. Negendank (2001), High-resolution geological record of historic earthquakes in the Dead Sea basin, *J. Geophys. Res.*, *106*, 2221–2234.

Kratinová, Z., P. Závada, F. Hrouda, and K. Schulmann (2006), Non-scaled analogue modelling of AMS development during viscous flow: A simulation on diapir-like structures, *Tectonophysics*, *418*(1–2), 51–61.

Lefort, J. P., T. Aïfa, and F. Hervé (2006), Structural and AMS study of a Miocene dyke swarm located above the Patagonian subduction, in *Dyke Swarms: Time Markers of Crustal Evolution*, edited by E. Hanski et al., pp. 225–241, Taylor and Francis, Philadelphia, Pa.

Levi, T., R. Weinberger, T. Aïfa, Y. Eyal, and S. Marco (2006), Earthquake-induced clastic dikes detected by anisotropy of magnetic susceptibility, *Geology*, *34*, 69–72, doi:10.1130/G-22001.1.

Liu, B., Y. Saito, T. Yamazaki, A. Abdeldayem, H. Oda, K. Hori, and Q. Zhao (2001), Paleocurrent analysis for the Late Pleistocene-Holocene incised-valley fill of Yangtze delta, China by using anisotropy of magnetic susceptibility data, *Mar. Geol.*, *176*, 175–189.

Marco, S., and A. Agnon (1995), Prehistoric earthquake deformation near Masada, Dead Sea graben, *Geology*, *23*, 695–698.

Marco, S., H. Ron, M. O. McWilliams, and M. Stein (1998), High-resolution record of geomagnetic secular variation from Late Pleistocene Lake Lisan sediments (paleo Dead Sea), *Earth Planet. Sci. Lett.*, *161*, 145–160.

McCalpin, J. P., (Ed.) (1996), *Paleoseismology*, *Int. Geophys. Ser.*, vol. 62, 588 pp., Elsevier, New York.

Mohindra, R., and T. N. Bagati (1996), Seismically induced soft-sediment deformation structures (seismites) around Sumdo in the lower Spiti valley (Tethys Himalaya), *Sediment. Geol.*, *101*, 69–83.

Moreira, M., L. Geoffroy, and J. P. Pozzi (1999), Ecoulement magnetique dans les dykes du point chaud des Açores: Etude préliminaire par anisotropie de susceptibilité magnétique (ASM) dans l'circ;le de San Jorge, *C. R. Acad. Sci., Ser. II*, *329*, 15–22.

Moretti, M. (2000), Soft-sediments deformation structures interpreted as seismites in middle-late Pleistocene Aeolian deposits (Apulian foreland, southern Italy), *Sediment. Geol.*, *135*, 167–179.

Nagata, T. (1961), *Rock Magnetism*, 350 pp., Maruzen, Tokyo.

Parés, J. M., and B. A. van der Pluijm (2003), Magnetic fabric and strain in pencil structures of the Knobs Formation, Valley and Rudge Province, US Appalachians, *J. Struct. Geol.*, *25*, 1349–1358.

Parés, J. M., B. A. van der Pluijm, and J. D. Turell (1999), Evolution of magnetic fabrics during incipient deformation of mudrocks (Pyreness, northern Spain), *Tectonophysics*, *307*, 1–14.

Paterson, S. R., T. K. Fowler, K. L. Schmidt, A. S. Yoshinobu, E. S. Yuan, and R. B. Miller (1998), Interpreting magmatic fabric patterns in plutons, *Lithos*, *44*, 53–82.

Poland, M. P., J. H. Fink, and L. Tauxe (2004), Patterns of magma flow in segmented silicic dikes at Summer Coon volcano, Colorado: AMS and thin section analysis, *Earth Planet. Sci. Lett.*, *219*, 155–169.

Quennell, A. M. (1959), The structural and geomorphic evolution of the Dead Sea Rift, *Q. J. Geol. Soc. London*, *114*, 1–24.

Rees, A. I. (1979), The orientation of grains in a sheared dispersion, *Tectonophysics*, *55*, 275–287.

Rees, A. I., and W. A. Woodall (1975), The magnetic fabric of some laboratory-deposited sediments, *Earth Planet. Sci. Lett.*, *25*, 121–130.

Rodríguez-Pascua, M. A., J. P. Calvo, G. De Vicente, and D. Gómez-Gras (2000), Soft-sediment deformation structures interpreted as seismites in lacustrine sediments of the Prebetic Zone, SE Spain, and their potential use as indicators of earthquake magnitudes during the Late Miocene, *Sediment. Geol.*, *135*, 117–135.

Sanin, F. D. (2002), Effect of solution physical chemistry on the rheological properties of activated sludge, *Water SA*, *28*(2), 207–211.

Schwehr, K., and L. Tauxe (2003), Characterization of soft-sediment deformation: Detection of cryptoslumps using magnetic methods, *Geology*, *31*, 203–206.

Shapira, A. (1997), Seismicity patterns of the Dead Sea Transform—A review, in *13th GIF Meeting on The Dead Sea Rift as a Unique Global Site*, Schriften der Alfred-Wegener-Stiftung, Terra Nostra, 4/97, Geophys. Inst. of Isr., Lod, Israel.

Shapira, A., R. Avni, and A. Nur (1993), A new estimate for the epicenter of the Jericho earthquake of 11 July 1927, *Isr. J. Earth Sci.*, *42*(2), 93–96.

Tarling, D. H., and F. Hrouda (1993), *The Magnetic Anisotropy of Rocks*, 217 pp., CRC Press, Boca Raton, Fla.

Tauxe, L. (1998), *Paleomagnetic Principles and Practice*, 299 pp., Springer, New York.

Turcotte, D. L., and G. Schubert (1982), *Geodynamics: Application of Continuum Physics to Geological Problems*, 450 pp., John Wiley, Hoboken, N. J.

Weinberger, R., G. Baer, G. Shamir, and A. Agnon (1995), Deformation bands associated with dike propagation in porous sandstone. Makhtesh Ramon, Israel, in *Physics and Chemistry of Dykes*, edited by G. Baer and A. Heimann, pp. 95–112, A. A. Balkema, Brookfield, Vt.

Weinberger, R., V. Lyakhovsky, G. Baer, and Z. B. Begin (2006a), Mechanical modeling and InSAR measurements of Mount Sedom uplift, Dead Sea basin: Implications for effective viscosity of rock salt, *Geochem. Geophys. Geosyst.*, *7*, Q05014, doi:10.1029/2005GC001185.

Weinberger, R., Z. B. Begin, N. Waldmann, M. Gardosh, G. Baer, A. Frumkin, and S. Wdowinski (2006b), Quaternary rise of the Sedom diapir, Dead Sea basin, in *New Frontiers in Dead Sea Paleoenvironmental Research*, edited by Y. Enzel, A. Agnon, and M. Stein, *Spec. Pap. Geol. Soc. Am.*, *401*, 33–51.

Zak, I. (1967), The geology of Mount Sedom (in Hebrew), Ph.D. thesis, Hebrew Univ., Jerusalem.